




 Cite this: *RSC Adv.*, 2018, 8, 13167

# Adsorbing the magnetic superhalogen $\text{MnCl}_3$ to realize intriguing half-metallic and spin-gapless-semiconducting behavior in zigzag or armchair SiC nanoribbon†

 Hui Li, Guangtao Yu, \* Zengsong Zhang, Yanfeng Ma, Xuri Huang and Wei Chen \*

By means of first-principles computations, we first propose a new and effective strategy through adsorbing the magnetic superhalogen  $\text{MnCl}_3$  to modulate the electronic and magnetic properties of zigzag- and armchair-edged SiC nanoribbons (zSiCNR and aSiCNR, respectively). In view of its large intrinsic magnetic moment and strong electron-withdrawing ability, the adsorption of magnetic superhalogen  $\text{MnCl}_3$  can introduce magnetism in the substrate SiCNR, and simultaneously induce the electron transfer process from SiCNR to  $\text{MnCl}_3$ , resulting in the evident increase of electrostatic potential in the ribbon plane, like applying an electric field. As a result, the magnetic degeneracy of pristine zSiCNR can be broken and a robust ferromagnetic half-metallicity or metallicity can be observed in the modified zSiCNR systems, while a robust ferromagnetic half-metallic or spin-gapless-semiconducting behavior can be obtained in the modified aSiCNR systems. Note that both the appealing half-metallicity and spin-gapless-semiconductor behavior are key features which hold promise for future spintronic applications. Moreover, all of these new superhalogen–SiC nanosystems can possess considerably high structural stabilities. These intriguing findings will be advantageous for promoting excellent SiC-based nanomaterials in the applications of spintronics and multifunctional nanodevices in the near future.

 Received 24th February 2018  
Accepted 19th March 2018

DOI: 10.1039/c8ra01632a

[rsc.li/rsc-advances](http://rsc.li/rsc-advances)

## 1 Introduction

The discovery of isolated graphene, an extended honeycomb network of  $\text{sp}^2$ -hybridized carbon atoms, has totally refreshed our minds and opened the gate to low dimensional nanomaterials.<sup>1,2</sup> Owing to its reduced dimensions, graphene can possess many fascinating physical properties,<sup>3–5</sup> such as massless Dirac Fermion behavior,<sup>3</sup> high mobility,<sup>4</sup> and the largest strength measured so far.<sup>5</sup> Inspired by these captivating properties, great effort has been made not only for graphene-based materials, but also for analogous inorganic materials.<sup>6–18</sup>

The inorganic SiC nanoribbon (SiCNR), as a structural analogue to graphene nanoribbon (GNR), has become a rising star in the family of inorganic nanomaterials, and is attracting great interest from many experimental and theoretical research groups. It is well known that SiC as a leading material can be extensively applied in harsh environments (*e.g.* high temperature, pressure or power),<sup>19–22</sup> since it possesses numerous outstanding characteristics, such as a large mechanical

strength, high thermal conductivity, as well as excellent resistance to oxidation and corrosion.<sup>23–26</sup> Experimentally, different polymorphs of SiC nanoribbons have been synthesized *via* several routes.<sup>27–31</sup> For example, *via* a catalyst-free route at a relatively low growth temperature, wurtzite-type SiC (2H–SiC) nanoribbons have been fabricated,<sup>27</sup> which are tens to hundreds of microns in length, a few microns in width and tens of nanometers in thickness. By a lithium-assisted synthetic route or the thermal evaporation approach, SiC (3C–SiC) nanoribbons have been obtained.<sup>28</sup> In addition, through the nanosecond pulsed laser direct-write and doping (LDWD) technique, carbon-rich SiC nanoribbons have been fabricated, which are proposed as transistor–resistor interconnects for nanodevices and photonic band-gap arrays in microstrip circuits.<sup>29</sup>

Besides, considerable theoretical work has been focused on one-dimensional (1D) inorganic SiCNRs with a zigzag or armchair edge. By means of first principles calculations, the ground state of zigzag SiCNR (zSiCNR) is predicted to be energetically degenerate with ferromagnetic (FM) and antiferromagnetic (AFM) configurations, where the metallic and half-metallic behaviors can be observed, respectively.<sup>32</sup> However, due to the magnetic degeneracy, the FM metallicity and AFM half-metallicity in pristine zSiCNR are vulnerable to even small disturbances, inhibiting its practical application in spintronics and multifunctional nanodevices. Comparatively, armchair

Laboratory of Theoretical and Computational Chemistry, Institute of Theoretical Chemistry, International Joint Research Laboratory of Nano-Micro Architecture Chemistry, Jilin University, Changchun 130023, People's Republic of China. E-mail: [yugt@jlu.edu.cn](mailto:yugt@jlu.edu.cn); [w\\_chen@jlu.edu.cn](mailto:w_chen@jlu.edu.cn)

† Electronic supplementary information (ESI) available. See DOI: 10.1039/c8ra01632a



SiCNR (aSiCNR) can exhibit nonmagnetic semiconducting behavior with a band gap of about 2.373 eV,<sup>33,34</sup> and such a large band gap is also not advantageous for its application in functional nanodevices.<sup>35,36</sup> To conquer these bottlenecks, some approaches have been proposed to modulate the electronic and magnetic properties of zSiCNR and aSiCNR systems,<sup>37–43</sup> for example, hydrogenation,<sup>37</sup> applying an electric field,<sup>38,39</sup> edge modification with functional groups/atoms,<sup>40,41</sup> and (non)covalent surface modification with an appropriate molecule/polymer.<sup>42,43</sup>

Differing from previously reported approaches, in this work we propose a new and effective strategy through adsorbing a magnetic superhalogen to tune the electronic and magnetic properties of zigzag- and armchair-edged SiC nanoribbons. It is well known that a superatom is a stable assembly of atoms that mimics the behavior of elemental atoms, and could serve as potential building blocks for the assembly of new materials with desired properties.<sup>44–52</sup> As one of the most important members in the family of superatoms, the superhalogens can possess larger electron affinities (EAs) than the halogen atoms, and have been extensively used in the design of novel materials.<sup>50–52</sup>  $\text{Mn}_x\text{Cl}_y$  can be considered as a unique moiety of the superhalogen group, and has been recently studied theoretically and synthesized experimentally.<sup>53,54</sup> Here, the magnetic superhalogen  $\text{MnCl}_3$  has been sampled to modulate the electronic and magnetic behaviors of SiCNR. We can understand that neutral  $\text{MnCl}_3$  possesses a considerable spin magnetic moment (*ca.* 4.00  $\mu_B$ ) and a large electron affinity (*ca.* 4.94 eV), even larger than that of the Cl atom (3.62 eV).<sup>55</sup> Thus, we can reasonably speculate that adsorbing  $\text{MnCl}_3$  could induce an evident change in electrostatic potential and simultaneously introduce magnetism to the substrate SiCNR, in view of the strong electron-withdrawing ability and intrinsic magnetic moment. It is highly anticipated that the adsorption of the magnetic superhalogen  $\text{MnCl}_3$  can effectively engineer the band structure of SiCNR, and so obtain captivating electronic and magnetic properties such as half-metallicity<sup>40</sup> and spin gapless semiconductor (SGS),<sup>37,56</sup> both of which are key features which hold promise for future spintronics applications.

In this study, we have carried out systematic density functional theory computations to investigate the structures, and the electronic and magnetic properties of zigzag- and armchair-edged SiCNR systems by adsorbing the magnetic superhalogen  $\text{MnCl}_3$ . We will mainly address the following issues: (1) can the adsorption of  $\text{MnCl}_3$  effectively tune the electronic and magnetic properties of zSiCNR and aSiCNR, and can the intriguing half-metallic or SGS behaviors be obtained? (2) How will the electronic and magnetic properties of modified zSiCNR or aSiCNR systems be affected when moving  $\text{MnCl}_3$  from the ribbon center to the edge? (3) Can the ribbon width have an impact on the electronic and magnetic behaviors of modified SiCNR systems? (4) How about the adsorption energies when depositing the magnetic superhalogen  $\text{MnCl}_3$  on the surface of SiCNRs? Undoubtedly, resolving these interesting issues will be advantageous for promoting the practical applications of excellent SiC-based nanomaterials in spintronics and multifunctional nanodevices.

## 2 Computational methods

All calculations are performed within the framework of density functional theory (DFT) as implemented in the Vienna *Ab initio* Simulation Package (VASP).<sup>57–60</sup> The electron–ion interaction is described by a projector augmented wave (PAW)<sup>61</sup> method using Perdew–Burke–Ernzerhof (PBE)<sup>62</sup> with van der Waals (vdw) correction proposed by Grimme (DFT-D2).<sup>63</sup> Vacuum regions of 15 Å along the non-periodic directions are used to avoid interaction of the periodic images. For the modified SiCNR systems with one  $\text{MnCl}_3$  in the supercell, there are five and three repeated units along the ribbon length for the corresponding substrates zSiCNR and aSiCNR. Moreover, a plane wave basis with a kinetic energy cutoff of 500 eV is used, which is found to yield well-converged total energies.  $1 \times 1 \times 11$  Monkhorst–Pack grid *k*-points are employed for the geometric relaxation, and the total energy convergence threshold is set as  $10^{-4}$  eV. On the basis of equilibrium structures, 21 *k*-points between every two high symmetry *k*-points along the one-dimensional Brillouin zone are used to obtain the band structures.<sup>64</sup> The amount of electron transfer between the adsorbed  $\text{MnCl}_3$  and SiC nanoribbon is estimated from the Bader charge analysis.

The adsorption energy of  $\text{MnCl}_3$  on the surface of SiCNR is calculated according to the following expression:

$$E_{\text{ad}} = E_{\text{SiCNR}+\text{MnCl}_3} - (E_{\text{SiCNR}} + E_{\text{MnCl}_3})$$

where  $E_{\text{SiCNRs}+\text{MnCl}_3}$  is the total energy of the modified SiCNR system with  $\text{MnCl}_3$ ,  $E_{\text{SiCNR}}$  means the energy of pristine SiCNR, and  $E_{\text{MnCl}_3}$  is the energy of single  $\text{MnCl}_3$ . The negative value of  $E_{\text{ad}}$  reflects the exothermic (energetically favorable) process for adsorbing  $\text{MnCl}_3$  on the surface of SiCNR. The large absolute value of  $E_{\text{ad}}$  means there is a strong interaction between  $\text{MnCl}_3$  and SiCNR.

## 3 Results and discussion

### 3.1 The electronic and magnetic properties of pristine SiC nanoribbons

In this study, we have considered two types of SiC nanoribbon with different edge chiralities, namely zigzag SiCNR (zSiCNR) and armchair SiCNR (aSiCNR), as illustrated in Fig. 1a and c. According to convention, different widths of zSiCNRs and aSiCNRs can be denoted as  $N_z$ -zSiCNR and  $N_a$ -aSiCNR, respectively, where  $N_z$  or  $N_a$  is the number of parallel zigzag chains or dimer lines across the corresponding ribbon width (Fig. 1a and c). All of the studied SiCNRs are terminated by hydrogen atoms to passivate the dangling bond on the ribbon edge. We take 8-zSiCNR and 13-aSiCNR as prototype systems and investigate the effect of adsorbing the magnetic superhalogen  $\text{MnCl}_3$  upon the electronic and magnetic properties of zigzag- and armchair-edged SiCNR systems.

To make a comparison, we initially investigate the geometrical structures, and the electronic and magnetic properties of pristine 8-zSiCNR and 13-aSiCNR. Both spin-polarized and spin-unpolarized computations have been performed, where the ferromagnetic (FM), antiferromagnetic (AFM) and nonmagnetic



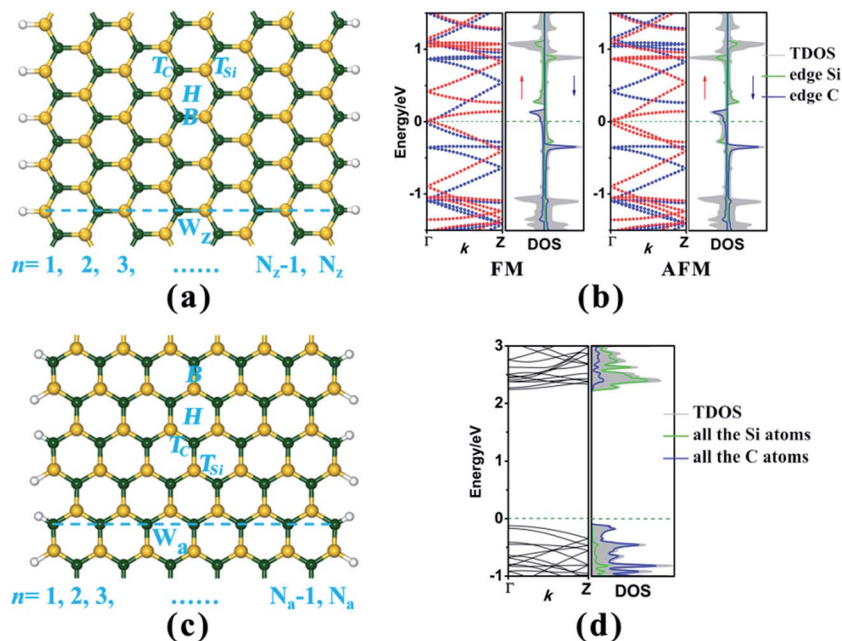


**Fig. 1** (a) The geometrical structure of H-terminated 8-zSiCNR. (b) The electronic band structures and corresponding DOS plots of pristine 8-zSiCNR in FM and AFM states, in which the red and blue dotted lines in the band structures represent the spin-up ( $\uparrow$ ) and spin-down ( $\downarrow$ ) channels, respectively. (c) The geometrical structure of H-terminated 13-aSiCNR. (d) The electronic band structure and corresponding DOS plot of pristine 13-aSiCNR in the NM state. The Fermi-level is set as zero and is indicated by a green dotted line. The yellow, dark green and white balls in the geometrical structures represent Si, C and H atoms, respectively.

(NM) states are considered. Our computed results reveal that for pristine 8-zSiCNR, the unpaired spin is mainly concentrated on the edge Si and C atoms, and their orientations are parallel and antiparallel between the Si and C edges for FM and AFM states respectively. Both the states are energetically degenerate, and yet much lower than the corresponding NM state, indicating that the degenerate FM and AFM configurations are the ground state of pristine zSiCNR. Furthermore, our computed band structures show that the pristine zSiCNR can exhibit metallic behavior in the FM state and half-metallic behavior in the AFM state. The computed results on the density of states (DOS) reveal that the FM metallicity can be dominated by spin-up and spin-down states across the Fermi-level mainly originating from the edge C and edge Si atoms, respectively, while the AFM half-metallicity can be determined by the spin-up states from the edge C and Si atoms crossing the Fermi-level (Fig. 1b).

Comparatively, our computed results reveal that pristine 13-aSiCNR is a nonmagnetic semiconductor with a direct band gap as large as 2.367 eV, where the top valence band (TVB) and bottom conduction band (BCB) are from the C and Si atoms, respectively (Fig. 1d). It is worth mentioning that all these computed results on pristine zSiCNR and aSiCNR are consistent with earlier reports.<sup>32–34</sup>

### 3.2 The geometrical structures, and electronic and magnetic properties of SiCNRs with the adsorbed $\text{MnCl}_3$ at the center

In this section we have performed a detailed investigation to explore the effect of adsorbing the magnetic superhalogen  $\text{MnCl}_3$  at the ribbon center upon the geometrical structures, and the electronic and magnetic properties of zigzag- and armchair-edged SiCNR systems, by sampling the corresponding

**Table 1** The relative energies  $\Delta E$  (meV) of different magnetic couplings to the ground state, the total magnetic moment  $M_{\text{tot}}$ , the distance  $d_{\text{Mn-C}}$  between the Mn atom in the adsorbed  $\text{MnCl}_3$  and the bonded C atom, the adsorption energy  $E_{\text{ad}}$ , the electronic property and the amount of electron transfer from SiCNR to  $\text{MnCl}_3$  for  $\text{MnCl}_3\text{-T}_\text{C}$ -8-zSiCNR-center and  $\text{MnCl}_3\text{-T}_\text{C}$ -13-aSiCNR-center

Systems	$\Delta E$ (meV)				$M_{\text{tot}}$ ( $\mu_B$ )	$d_{\text{Mn-C}}$ ( $\text{\AA}$ )	$E_{\text{ad}}$ (eV)	Electronic property	The charge of the SiCNR $ e $
	NM	FM	FM-1 <sup>a</sup>	AFM					
8-zSiNR	166.7	0.0	—	0.0	2.14/0.0	—	—	—	—
$\text{MnCl}_3\text{-T}_\text{C}$ -8-zSiCNR-center	—	0.0	31.6	—	7.10	2.281	−2.319	Metallicity	0.905
13-aSiCNR	0.0	—	—	—	—	—	—	Semiconductor <sup>b</sup>	—
$\text{MnCl}_3\text{-T}_\text{C}$ -13-aSiCNR-center	1.798	0.0	—	—	4.00	2.107	−1.430	Half-metallicity <sup>c</sup>	0.681

<sup>a</sup> FM-1 represents the parallel coupling between  $\text{MnCl}_3$  and the C-edge, accompanied by the antiparallel coupling between the Si and C edges. <sup>b</sup> The band gap is 2.367 eV. <sup>c</sup> The gap in the minority channel is 1.463 eV.



8-zSiCNR and 13-aSiCNR. Our computed results reveal that the sole  $\text{MnCl}_3$  possesses a large electron affinity (*ca.* 4.728 eV) and spin magnetic moment (*ca.*  $4.00 \mu_B$ ), consistent with those reported previously.<sup>53</sup> Consequently, adsorbing the magnetic superhalogen  $\text{MnCl}_3$ , with its strong electron-withdrawing ability as well as its intrinsic magnetic moment, could significantly change the electrostatic potential and simultaneously introduce magnetism to the substrate SiCNR. It is highly anticipated that this kind of surface modification by the appealing magnetic superhalogen unit can effectively modulate the electronic and magnetic behaviors for zigzag- and armchair-edged SiC nanoribbons, promoting the practical application of SiC-based nanomaterials in multifunctional and spintronic nanodevices.

Initially, we focus on the adsorption of  $\text{MnCl}_3$  at the ribbon center for 8-zSiCNR and 13-aSiCNR, where all four possible adsorption sites for the Mn atom are considered, including the top site of the C atom ( $T_C$ ), the top site of the Si atom ( $T_{Si}$ ), the bridge site over the Si-C bond (B) and the hollow site of the SiC hexagonal ring (H), as illustrated Fig. 1a and c. Note that these  $\text{MnCl}_3$ -modified 8-zSiCNR and 13-aSiCNR systems are named  $\text{MnCl}_3$ -8-zSiCNR-center and  $\text{MnCl}_3$ -13-aSiCNR-center, respectively, where “center” denotes that the adsorption site of  $\text{MnCl}_3$  is at the ribbon center. Our computed results reveal that  $\text{MnCl}_3$ - $T_C$ -8-zSiCNR-center and  $\text{MnCl}_3$ - $T_C$ -13-aSiCNR-center are the most stable among their respective possible zSiCNR or aSiCNR configurations with the adsorption of  $\text{MnCl}_3$  at the center, as discussed in detail in the ESI (Fig. S1 and S2†).

In these two stable  $\text{MnCl}_3$ - $T_C$ -8-zSiCNR-center and  $\text{MnCl}_3$ - $T_C$ -13-aSiCNR-center configurations, the original planar structure of  $\text{MnCl}_3$  can be deformed owing to the formation of a Mn-C bond (2.281 Å for the former and 2.107 Å for the latter). The computed adsorption energies are -2.319 eV and -1.430 eV respectively (Table 1), and such the large negative adsorption energy suggests that adsorbing the magnetic superhalogen  $\text{MnCl}_3$  on the surface of SiCNR can be an energetically favorable process, and that the resulting joint system can possess high structural stability.

Furthermore, we explore the effect of adsorbing  $\text{MnCl}_3$  upon the electronic and magnetic properties of pristine zigzag- and

armchair-edged SiCNRs. The computed results reveal that the adsorption of  $\text{MnCl}_3$  over the ribbon center can break the magnetic degeneracy of pristine zSiCNR, and that sole FM metallicity can be observed in  $\text{MnCl}_3$ - $T_C$ -8-zSiCNR-center (Fig. 2a and Table 1). The corresponding total magnetic moment  $M_{\text{tot}}$  is as large as  $7.10 \mu_B$  per supercell. Clearly, this approach can overcome the problem of FM metallicity and AFM half-metallicity being vulnerable to even small disturbances owing to the energy degeneracy of FM and AFM states for pristine zSiCNR, which is advantageous for promoting practical application in multifunctional nanodevices. The computed DOS results show that the metallicity in  $\text{MnCl}_3$ - $T_C$ -8-zSiCNR-center is mainly determined by the spin-up and spin-down states from the respective edge C and edge Si atoms across the Fermi level (Fig. 2a). Comparatively, adsorbing  $\text{MnCl}_3$  over the ribbon center of 13-aSiCNR can transform the original NM semiconductor such that it exhibits intriguing FM half-metallicity (Fig. 2b and Table 1), where the total magnetic moment  $M_{\text{tot}}$  is as large as  $4.00 \mu_B$  per supercell and the gap in the minority channel is as large as 1.463 eV. Such a large semiconducting spin gap suggests that the half-metallicity is rather robust and there is great potential for experimental realization.<sup>65</sup> Note that great effort has been made in exploring the half-metallicity in low-dimensional nanomaterials (*e.g.*, GNRs<sup>10,14</sup> and BNNRs<sup>66,67</sup>), in view of their potential application in spintronics. Moreover, the computed DOS results reveal that the half-metallic behavior in  $\text{MnCl}_3$ - $T_C$ -13-aSiCNR-center can be mainly dominated by the spin-down state crossing the Fermi level from  $\text{MnCl}_3$  and C atoms (Fig. 2b).

To understand the reason why adsorbing superhalogen  $\text{MnCl}_3$  can effectively engineer the band structures of pristine zSiCNR and aSiCNR, we have performed computations on the electrostatic potential and Bader charge for the two most stable conformations, namely,  $\text{MnCl}_3$ - $T_C$ -8-zSiCNR-center and  $\text{MnCl}_3$ - $T_C$ -13-aSiCNR-center. As illustrated in Fig. 3, independent of the edge chirality, the substrate SiCNR in the modified system can possess a different distribution of electrostatic potential from that of pristine SiCNR, where the adsorption of strong electron-withdrawing  $\text{MnCl}_3$  can induce an increase of electrostatic potential in the substrate of SiCNR. This situation can be due to

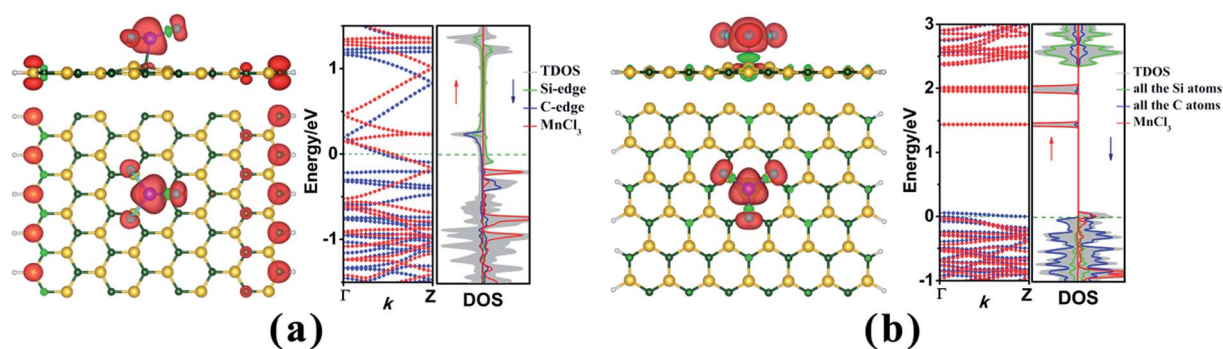


Fig. 2 The geometry, electron spin density distribution, band structure and corresponding DOS for the most favorable SiCNR-based configurations with adsorbed  $\text{MnCl}_3$  at the ribbon center, namely, (a)  $\text{MnCl}_3$ - $T_C$ -8-zSiCNR-center and (b)  $\text{MnCl}_3$ - $T_C$ -13-aSiCNR-center. The red and green colors in the electron spin density distribution represent the spin-up and spin-down orientations of the unpaired electrons, respectively. The red and blue dotted lines in the band structures denote the spin-up ( $\uparrow$ ) and spin-down ( $\downarrow$ ) channels, respectively. The Fermi-level is set as zero and is indicated by the green dotted line.



the occurrence of electron transfer from the substrate (*ca.*  $0.905|e|$  and  $0.681|e|$  for 8-zSiCNR and 13-aSiCNR, respectively) to  $\text{MnCl}_3$  (Table 1). Obviously, the adsorption of superhalogen  $\text{MnCl}_3$  can result in an evident change of electrostatic potential in SiCNR, just like applying an electric field, which is mainly responsible for engineering the band structures of zigzag- and armchair-edged SiCNRs. It is worth mentioning that when applying an external electric field, the magnetic degeneracy of zSiCNR can be broken and that sole FM metallic behavior can be observed,<sup>38</sup> while the band gap of aSiCNR can be decreased with an increase of field strength and even metallic behavior can be obtained.<sup>39</sup>

Clearly, adsorbing the magnetic superhalogen  $\text{MnCl}_3$  at the ribbon center can effectively modulate the electronic and magnetic behaviors of SiCNR with the zigzag or armchair edge. The magnetic degeneracy of pristine zSiCNR can be broken and sole FM metallicity can be achieved, while the NM semiconductor of aSiCNR can be changed so as to exhibit a robust FM half-metallicity. These intriguing findings will be advantageous for promoting the practical application of SiC-based nanomaterials in multifunctional and spintronic nanodevices.

### 3.3 The geometrical structures, and the electronic and magnetic properties of SiCNRs with the adsorbed $\text{MnCl}_3$ at the ribbon edge

Based on the above discussion, we can understand that adsorbing the magnetic superhalogen  $\text{MnCl}_3$  over the ribbon

center can effectively modulate the electronic and magnetic properties of SiC nanoribbons, such that FM metallicity and FM half-metallicity can be observed in the modified zSiCNR and aSiCNR systems, respectively. In this section, we will explore the effect of moving  $\text{MnCl}_3$ , from the ribbon center to the edge, on the electronic and magnetic properties of zigzag- and armchair-edged SiCNRs. It is well known that nanoribbon edges are more chemically active, thus it is highly anticipated that adsorbing  $\text{MnCl}_3$  at the edge can also effectively engineer the band structures of SiCNRs and even induce intriguing electronic and magnetic properties such as half-metallic and SGS behaviors, both of which are key features which hold promise for future spintronic applications.

Initially, we take the most stable  $\text{MnCl}_3\text{-T}_\text{C}\text{-8-zSiCNR-center}$  and  $\text{MnCl}_3\text{-T}_\text{C}\text{-13-aSiCNR-center}$  systems with  $\text{MnCl}_3$  adsorbed at the center as the starting points to examine the effect of the adsorption site upon the electronic and magnetic properties of zSiCNR and aSiCNR by moving  $\text{MnCl}_3$  from the ribbon center to the edge, where the Mn atom is still located atop the C atom. As shown in Fig. 4a and b, while changing the position of  $\text{MnCl}_3$  towards the Si/C edge of zSiCNR, two corresponding conformations  $\text{MnCl}_3\text{-T}_\text{C}\text{-8-zSiCNR-eSi}$  and  $\text{MnCl}_3\text{-T}_\text{C}\text{-8-zSiCNR-eC}$  can be obtained, where “eSi” and “eC” mean the adsorption site of  $\text{MnCl}_3$  located at the Si edge and C edge, respectively. Similarly, when moving  $\text{MnCl}_3$  to the edge of aSiCNR, we can obtain one new configuration  $\text{MnCl}_3\text{-T}_\text{C}\text{-13-aSiCNR-edge}$  (Fig. 4c), where the “edge” means the adsorption site located at the edge of

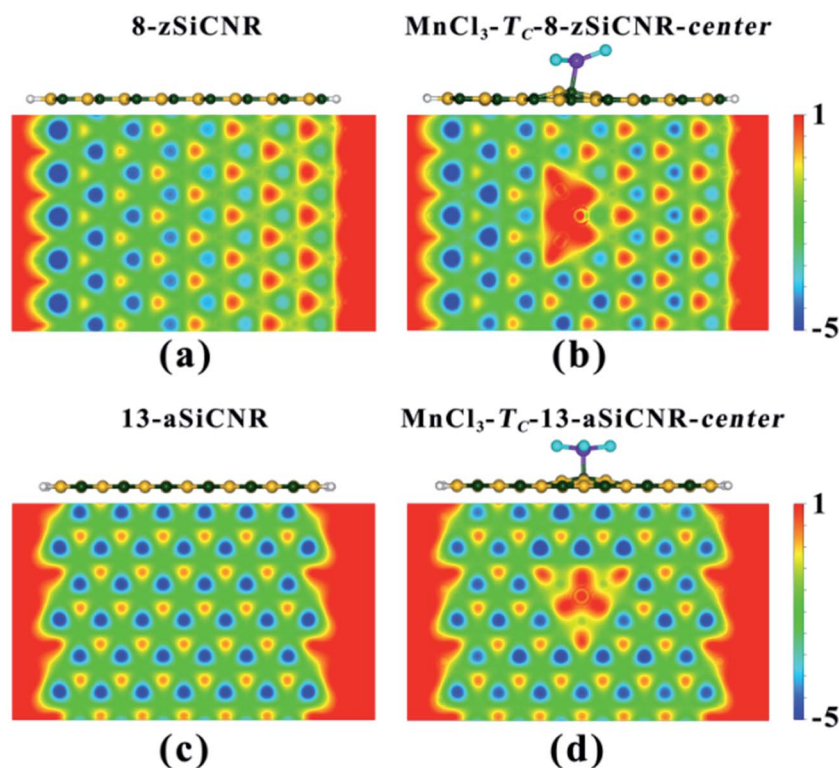


Fig. 3 The side view of the geometrical structure and the distribution of electrostatic potential in the nanoribbon plane for the pristine SiCNRs and the corresponding  $\text{MnCl}_3$ -modified SiCNR systems at the center: (a) pristine 8-zSiCNR, (b)  $\text{MnCl}_3\text{-T}_\text{C}\text{-8-zSiCNR-center}$ , (c) pristine 13-aSiCNR and (d)  $\text{MnCl}_3\text{-T}_\text{C}\text{-13-aSiCNR-center}$ .



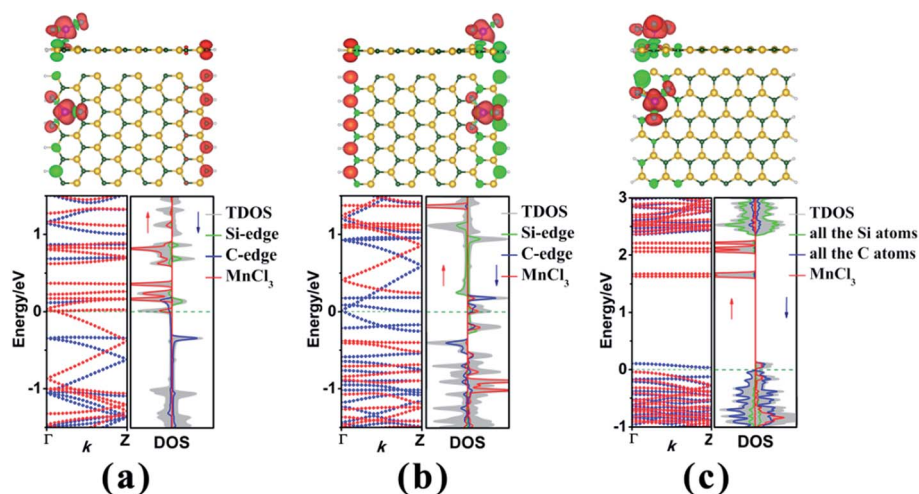


Fig. 4 The geometry, electron spin density distribution, band structure and corresponding DOS for the  $\text{MnCl}_3$ -modified SiCNr systems at the ribbon edge, namely, (a)  $\text{MnCl}_3\text{-Tc-8-zSiCNr-eSi}$ , (b)  $\text{MnCl}_3\text{-Tc-8-zSiCNr-eC}$  and (c)  $\text{MnCl}_3\text{-Tc-13-aSiCNr-edge}$ . The red and green colors in the electron spin density distribution represent the spin-up and spin-down orientations of the unpaired electrons, respectively. The red and blue dotted lines in the band structures denote the spin-up ( $\uparrow$ ) and spin-down ( $\downarrow$ ) channels, respectively. The Fermi-level is set as zero and is indicated by the green dotted line.

aSiCNr. Our computed results reveal that the distances between the Mn atom and the bonded C atom are 2.260, 2.175 and 2.179 Å for  $\text{MnCl}_3\text{-Tc-8-zSiCNr-eSi}$ ,  $\text{MnCl}_3\text{-Tc-8-zSiCNr-eC}$  and  $\text{MnCl}_3\text{-Tc-13-aSiCNr-edge}$ , respectively (Table 2). All of these three configurations with  $\text{MnCl}_3$  at the ribbon edge can possess considerable adsorption energies of  $-3.865$ ,  $-1.826$  and  $-1.719$  eV, respectively (Table 2). Particularly, the  $\text{MnCl}_3$ -modified zSiCNr at the Si edge and  $\text{MnCl}_3$ -modified aSiCNr at the ribbon edge can even possess larger absolute values than the corresponding ones with  $\text{MnCl}_3$  at the center, indicating that both of them are more stable in energy.

Subsequently, we explore the effect of the adsorption site upon the electronic and magnetic properties of these three  $\text{MnCl}_3$ -modified zSiCNr and aSiCNr systems by computing the band structures and DOSs, including  $\text{MnCl}_3\text{-Tc-8-zSiCNr-eSi}$ ,  $\text{MnCl}_3\text{-Tc-8-zSiCNr-eC}$  and  $\text{MnCl}_3\text{-Tc-13-aSiCNr-edge}$ . The computed results reveal that when changing the adsorption site of  $\text{MnCl}_3$  from the center to the Si edge of zSiCNr, the original metallicity can be transformed into half-metallicity (Fig. 4a and Table 2). Additionally, compared with the FM state (with the uniform parallel coupling between the  $\text{MnCl}_3$ , Si and C edges) of  $\text{MnCl}_3\text{-Tc-8-zSiCNr-center}$ ,  $\text{MnCl}_3\text{-Tc-8-zSiCNr-eSi}$  can also exhibit a large total magnetic moment ( $M_{\text{tot}} = 6.00 \mu_{\text{B}}$ ), where

the spin distribution is parallel between  $\text{MnCl}_3$  and the C edge, but antiparallel between the Si and C edges. Note that this kind of spin distribution can be also considered as the ferromagnetic state (denoted by FM-1), in view of the case that the total magnetic moment of the composite system is large, which can be mainly dominated by adsorbed  $\text{MnCl}_3$ .

Similarly, when moving  $\text{MnCl}_3$  from the center to the C edge of zSiCNr, a conversion of the metallicity to half-metallicity can be still achieved where the ferromagnetic state (FM-1) with a large total magnetic moment ( $M_{\text{tot}} = 4.00 \mu_{\text{B}}$ ) is also observed (Fig. 4b and Table 2). The computed DOS results reveal that the half-metallic behaviors in  $\text{MnCl}_3\text{-Tc-8-zSiCNr-eSi}$  and  $\text{MnCl}_3\text{-Tc-8-zSiCNr-eC}$  can be dominated by the spin-up states and spin-down states crossing the Fermi level, respectively, both of which uniformly originate from the edge Si/C atoms and  $\text{MnCl}_3$ , as illustrated in Fig. 4a and b. Clearly, adsorbing the magnetic superhalogen  $\text{MnCl}_3$  at the Si/C edge can also break the magnetic degeneracy of zSiCNr, owing to the evident electron transfer (*ca.* 0.888 and 0.755 $|e|$ , respectively) from zSiCNr to  $\text{MnCl}_3$  leading to an increase of electrostatic potential in the nanoribbon plane (Table 2 and Fig. 5). The robust half-metallic behavior can be uniformly observed in the two modified cases, where the semiconducting spin gaps of the minority channel

Table 2 The relative energies  $\Delta E$  (meV) of different magnetic couplings to the ground state, the total magnetic moment  $M_{\text{tot}}$ , the distance  $d_{\text{Mn-C}}$  between the Mn atom in the adsorbed  $\text{MnCl}_3$  and the bonded C atom, the adsorption energy  $E_{\text{ad}}$ , the electronic property and the amount of the electron transfer from SiCNr to  $\text{MnCl}_3$  for the modified zSiCNr and aSiCNr systems with the  $\text{MnCl}_3$  at the ribbon edge

Systems	$\Delta E$ (meV)			$M_{\text{tot}}$ ( $\mu_{\text{B}}$ )	$d_{\text{Mn-C}}$ (Å)	$E_{\text{ad}}$ (eV)	Electronic property	The gap in the minority channel (eV)	The charge of the SiCNr $ e $
	NM	FM	FM-1						
$\text{MnCl}_3\text{-Tc-8-zSiCNr-eSi}$	—	5.1	0.0	6.00	2.260	$-3.865$	Half-metallicity	0.450	0.888
$\text{MnCl}_3\text{-Tc-8-zSiCNr-eC}$	—	139.5	0.0	4.00	2.175	$-1.826$	Half-metallicity	0.622	0.755
$\text{MnCl}_3\text{-Tc-13-aSiCNr-edge}$	1.939	0.0	—	4.00	2.179	$-1.719$	SGS	—	0.723



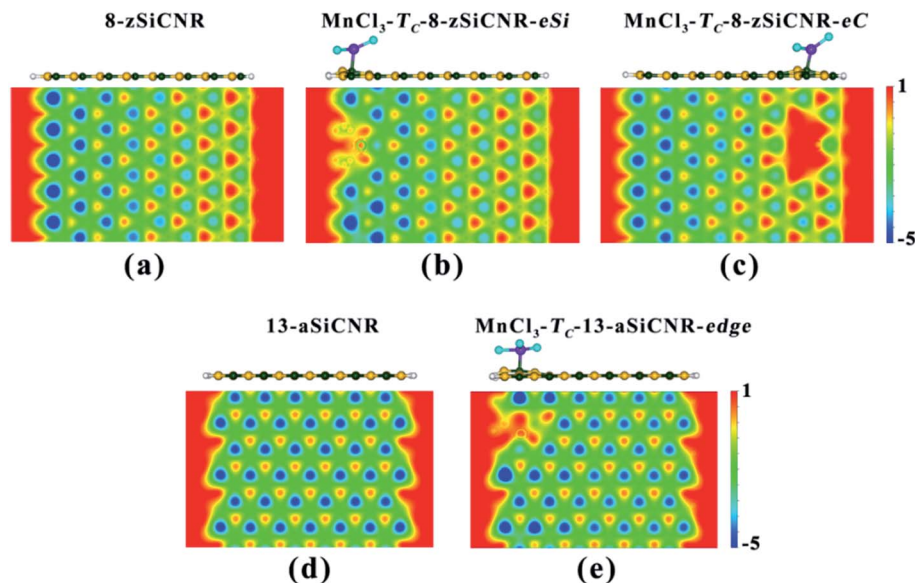


Fig. 5 The side view of the geometrical structure and the distribution of electrostatic potential in the nanoribbon plane for the pristine SiCNRs and the corresponding  $\text{MnCl}_3$ -modified SiCNR systems at the edge: (a) pristine 8-zSiCNR, (b)  $\text{MnCl}_3\text{-T}_\text{C}$ -8-zSiCNR-eSi, (c)  $\text{MnCl}_3\text{-T}_\text{C}$ -8-zSiCNR-eC, (d) pristine 13-aSiCNR and (e)  $\text{MnCl}_3\text{-T}_\text{C}$ -13-aSiCNR-edge.

are considerably large (0.450 and 0.622 eV, respectively), as shown in Table 2 and Fig. 4.

Comparatively, when moving  $\text{MnCl}_3$  from the center to the edge of 13-aSiCNR, the FM ground state ( $M_\text{tot} = 4.00 \mu_\text{B}$ ) can be maintained, yet the original half-metallicity can be converted into an intriguing SGS behavior, where both the top valence band from the C atoms and the bottom conduction band from the C atoms and  $\text{MnCl}_3$  are in contact with each other at the Fermi-level, as illuminated in Fig. 4c. Evidently, adsorbing the superhalogen  $\text{MnCl}_3$  at the edge can effectively engineer the band structure of aSiCNR, due to the obvious electron transfer (ca.  $0.723|e|$ ) from aSiCNR to  $\text{MnCl}_3$  leading to an increase of electrostatic potential in the nanoribbon plane (Table 2 and Fig. 5e).

Overall, adsorbing the magnetic superhalogen  $\text{MnCl}_3$  at the edge can also effectively tune the electronic and magnetic properties of zigzag- and armchair-edged SiCNRs, in which steady ferromagnetic half-metallic or SGS behaviors can be achieved. This can be advantageous for promoting the practical application of SiC-based nanomaterials in spintronics.

### 3.4 The geometrical structures, and the electronic and magnetic properties of $\text{MnCl}_3$ -modified SiCNR systems with different widths

It is well known that the half-metallic and SGS behaviors in low-dimensional nanostructures have attracted great attention from researchers,<sup>37,40,56</sup> owing to their promising application in spintronics. From the above discussion, we can understand that half-metallic and SGS behaviors can be observed in  $\text{MnCl}_3$ -modified 8-zSiCNR and 13-aSiCNR systems at the ribbon edge, respectively. In this section, we ask whether both intriguing characteristics can be sustained when changing the ribbon width of correlative composite systems. We examined the effect of ribbon width ( $N_\text{z}$  or  $N_\text{a}$ ) upon the electronic and magnetic properties of the representative  $\text{MnCl}_3$ -modified zSiCNR system at the Si edge (more favorable in energy) and the  $\text{MnCl}_3$ -modified aSiCNR system at the ribbon edge by sampling  $N_\text{z} = 6, 10, 12$  and  $N_\text{a} = 9, 11, 15$ , respectively, where the adsorption site of  $\text{MnCl}_3$  is kept atop the C atom. For convenience, these systems can be denoted as  $\text{MnCl}_3\text{-T}_\text{C}\text{-}N_\text{z}\text{-zSiCNR-eSi}$  or  $\text{MnCl}_3\text{-T}_\text{C}\text{-}N_\text{a}\text{-aSiCNR-edge}$ .

Table 3 The relative energies  $\Delta E$  (meV) of different magnetic couplings to the ground state, the total magnetic moment  $M_\text{tot}$ , the distance  $d_\text{Mn-C}$  between the Mn atom in the adsorbed  $\text{MnCl}_3$  and the bonded C atom, the adsorption energy  $E_\text{ad}$ , the electronic property and the amount of the electron transfer from SiCNR to  $\text{MnCl}_3$  for the modified zSiCNR and aSiCNR systems with different widths

Systems	$\Delta E$ (meV)			$M_\text{tot}$ ( $\mu_\text{B}$ )	$d_\text{Mn-C}$ ( $\text{\AA}$ )	$E_\text{ad}$ (eV)	Electronic property	The gap in the minority channel (eV)	The charge of the SiCNR $ e $
	NM	FM	FM-1						
$\text{MnCl}_3\text{-T}_\text{C}\text{-6-zSiCNR-eSi}$	—	24.0	0.0	4.00	2.256	−3.788	Half-metallicity	0.516	0.849
$\text{MnCl}_3\text{-T}_\text{C}\text{-10-zSiCNR-eSi}$	—	7.3	0.0	6.00	2.270	−3.836	Half-metallicity	0.469	0.864
$\text{MnCl}_3\text{-T}_\text{C}\text{-12-zSiCNR-eSi}$	—	11.5	0.0	6.00	2.262	−3.915	Half-metallicity	0.520	0.899
$\text{MnCl}_3\text{-T}_\text{C}\text{-9-aSiCNR-edge}$	1.991	0.0	—	4.00	2.188	−1.730	SGS	—	0.779
$\text{MnCl}_3\text{-T}_\text{C}\text{-11-aSiCNR-edge}$	1.991	0.0	—	4.00	2.188	−1.680	SGS	—	0.763
$\text{MnCl}_3\text{-T}_\text{C}\text{-15-aSiCNR-edge}$	1.958	0.0	—	4.00	2.179	−1.683	SGS	—	0.742



Our computed results reveal that all of these  $\text{MnCl}_3$ -modified zSiCNR and aSiCNR systems with different ribbon widths can also possess considerable negative adsorption energies in the range of  $-3.788$  to  $-3.915$  eV and  $-1.680$  to  $-1.730$  eV, respectively, in which the distances between the Mn atom and the bonded C atom are in the range of  $2.179$ – $2.270$  Å, as shown in Table 3.

As illustrated in Table 3 and Fig. 6, we can find that when the ribbon width  $N_z$  is narrowed from 8 to 6, the half-metallic behavior with the ferromagnetic state (FM-1) can be maintained in the  $\text{MnCl}_3$ -modified zSiCNR system at the Si edge, in which the total magnetic moment  $M_{\text{tot}}$  is as large as  $4.00 \mu_B$ . The half-metallicity in  $\text{MnCl}_3$ - $T_C$ -6-zSiCNR-eSi can be mainly dominated by the edge C atoms in the spin-down channel across the Fermi level (Fig. 6a). Conversely, when widening the ribbon

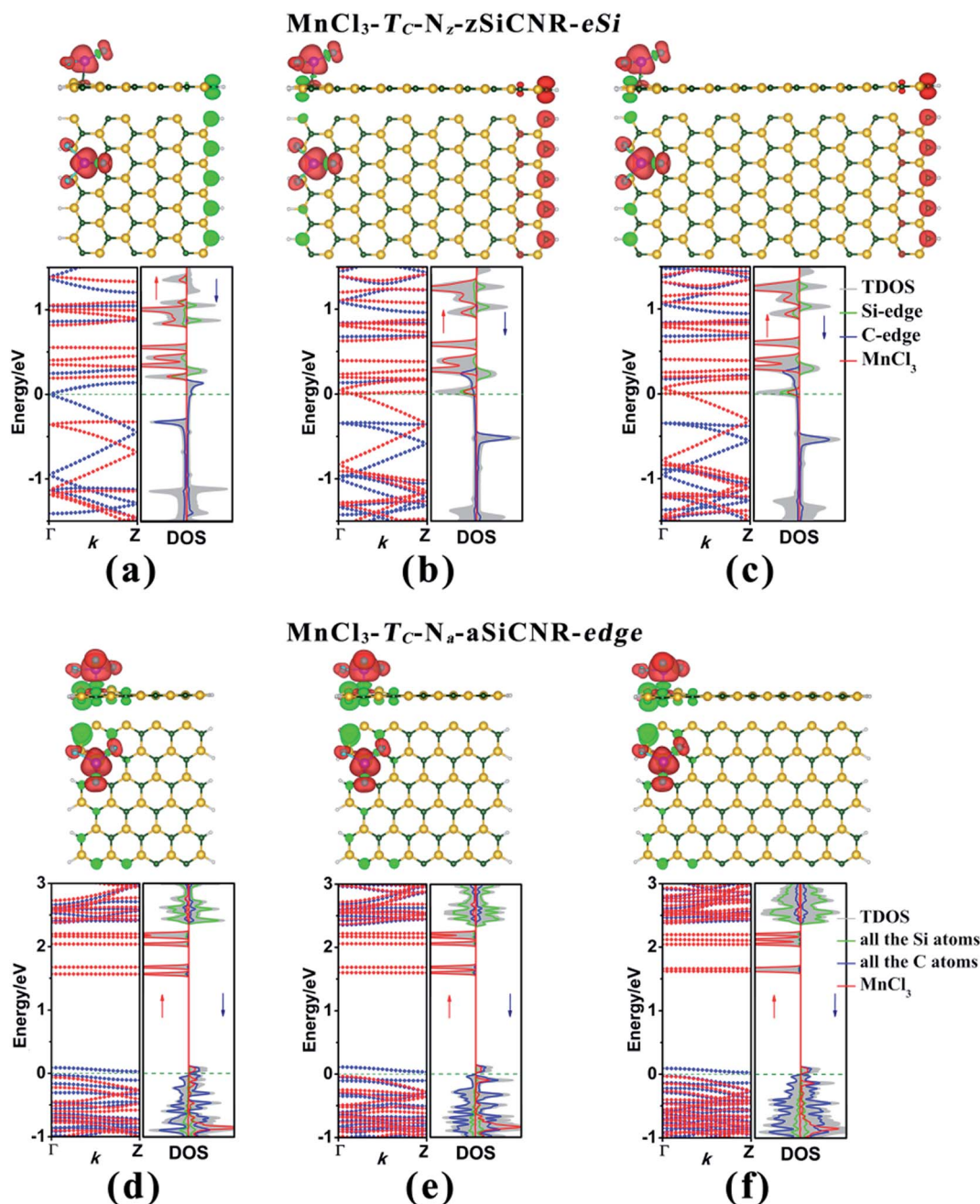


Fig. 6 The geometry, electron spin density distribution, band structure and corresponding DOS for the different widths of  $\text{MnCl}_3$ -modified SiCNR systems at the ribbon edge, namely, (a)  $\text{MnCl}_3$ - $T_C$ -6-zSiCNR-eSi, (b)  $\text{MnCl}_3$ - $T_C$ -10-zSiCNR-eSi, (c)  $\text{MnCl}_3$ - $T_C$ -12-zSiCNR-eSi, (d)  $\text{MnCl}_3$ - $T_C$ -9-aSiCNR-edge, (e)  $\text{MnCl}_3$ - $T_C$ -11-aSiCNR-edge and (f)  $\text{MnCl}_3$ - $T_C$ -15-aSiCNR-edge. The red and green colors in the electron spin density distribution represent the spin-up and spin-down orientations of the unpaired electrons, respectively. The red and blue dotted lines in the band structures denote the spin-up ( $\uparrow$ ) and spin-down ( $\downarrow$ ) channels, respectively. The Fermi-level is set as zero and is indicated by the green dotted line.



width  $N_z$  to 10 and even 12, the half-metallic behavior with the ferromagnetic state (FM-1,  $M_{\text{tot}} = 6.00 \mu_B$ ) can be still sustained in the  $\text{MnCl}_3$ -modified zSiCNR systems at the Si edge. The computed DOS results reveal that the half-metallicities in  $\text{MnCl}_3$ - $T_C$ -10-zSiCNR-eSi and  $\text{MnCl}_3$ - $T_C$ -12-zSiCNR-eSi can be uniformly determined by the spin-up states crossing the Fermi level from the edge Si/C atoms and  $\text{MnCl}_3$  (Fig. 6b and c). It is worth mentioning that all the half-metallic behaviors in these three configurations are also rather robust, where the semi-conducting spin gap of the minority channel is considerably large with a range of 0.469–0.520 eV (Table 3 and Fig. 6).

Similarly, when narrowing or widening the ribbon width  $N_a$  from 13 to 9, 11 and 15, the SGS behavior with FM ground state ( $M_{\text{tot}} = 4.00 \mu_B$ ) can be kept in the  $\text{MnCl}_3$ -modified aSiCNR

systems at the ribbon edge. The computed DOS results reveal that for all of these three systems, both the top valence band from C atoms and the bottom conduction band from the C atoms and  $\text{MnCl}_3$  are uniformly in contact with each other at the Fermi-level, resulting in SGS behavior, as illustrated in Fig. 6d–f.

Obviously, independent of the ribbon width, adsorbing the superhalogen  $\text{MnCl}_3$  can effectively engineer band structures of zigzag- and armchair-edged SiCNR systems, owing to the resulting increase of electrostatic potential in the ribbon plane (Fig. 7). The robust half-metallic and SGS behaviors can be maintained for different widths of  $\text{MnCl}_3$ -modified zSiCNR and aSiCNR systems at the edge, respectively. It is worth mentioning that we have also doubled the above used supercells to consider

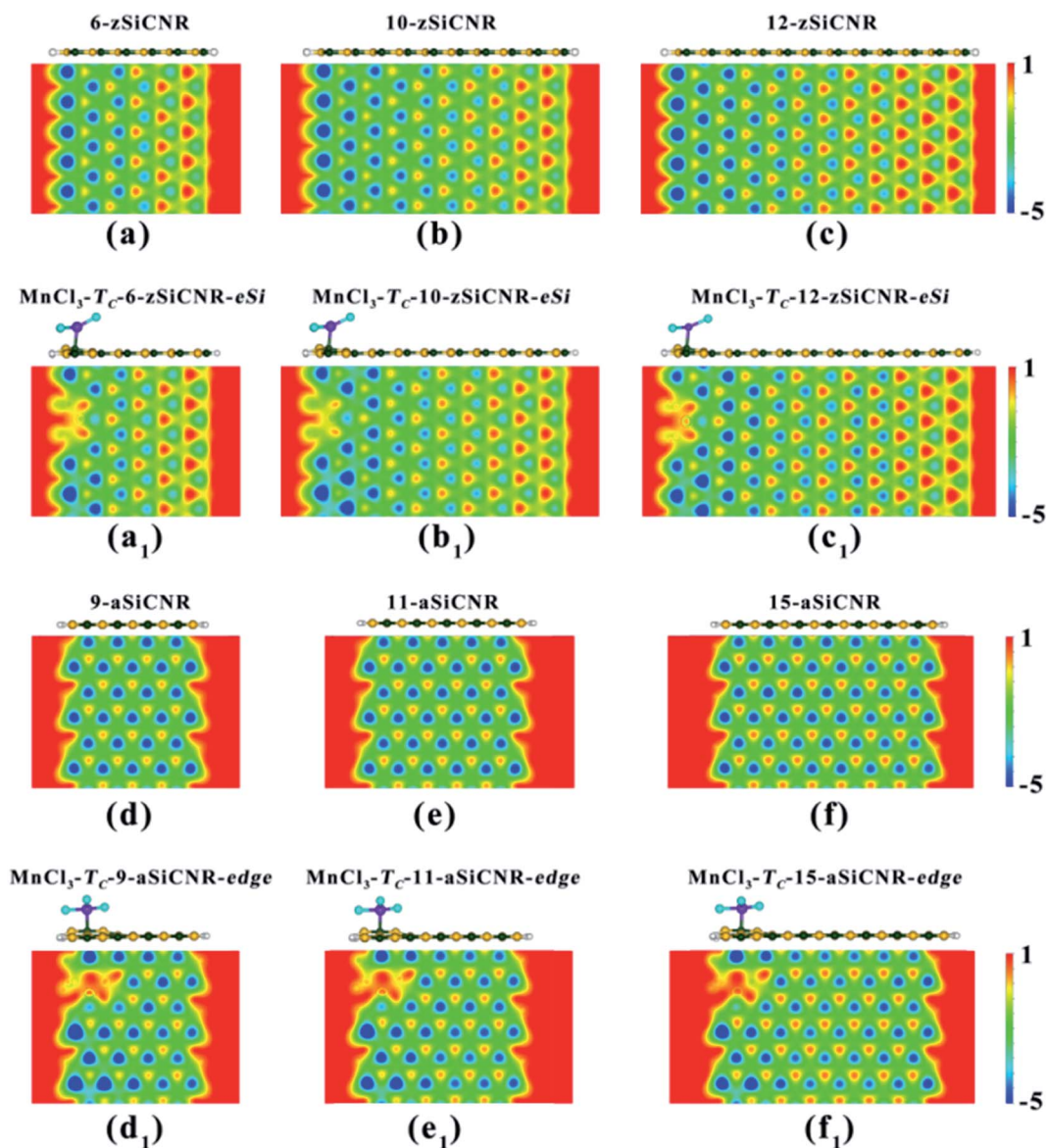


Fig. 7 The side view of the geometrical structure and the distribution of electrostatic potential in the nanoribbon plane for the pristine SiCNRs with different widths and the corresponding  $\text{MnCl}_3$ -modified SiCNR systems at the edge: (a) pristine 6-zSiCNR, (b) pristine 10-zSiCNR, (c) pristine 12-zSiCNR, (a<sub>1</sub>)  $\text{MnCl}_3$ - $T_C$ -6-zSiCNR-eSi, (b<sub>1</sub>)  $\text{MnCl}_3$ - $T_C$ -10-zSiCNR-eSi, (c<sub>1</sub>)  $\text{MnCl}_3$ - $T_C$ -12-zSiCNR-eSi, (d) pristine 9-aSiCNR, (e) pristine 11-aSiCNR, (f) pristine 15-aSiCNR, (d<sub>1</sub>)  $\text{MnCl}_3$ - $T_C$ -9-aSiCNR-edge, (e<sub>1</sub>)  $\text{MnCl}_3$ - $T_C$ -11-aSiCNR-edge and (f<sub>1</sub>)  $\text{MnCl}_3$ - $T_C$ -15-aSiCNR-edge.



the relative energies between the parallel and antiparallel couplings of two neighboring  $\text{MnCl}_3$  sites for the modified SiCNR systems, by sampling the representative systems including  $\text{MnCl}_3\text{-T}_\text{C}\text{-6-zSiCNR-eSi}$ ,  $\text{MnCl}_3\text{-T}_\text{C}\text{-8-zSiCNR-eSi}$ ,  $\text{MnCl}_3\text{-T}_\text{C}\text{-8-zSiCNR-center}$ ,  $\text{MnCl}_3\text{-T}_\text{C}\text{-8-zSiCNR-eC}$ , as well as  $\text{MnCl}_3\text{-T}_\text{C}\text{-9-aSiCNR-edge}$ ,  $\text{MnCl}_3\text{-T}_\text{C}\text{-11-aSiCNR-edge}$ ,  $\text{MnCl}_3\text{-T}_\text{C}\text{-13-aSiCNR-edge}$  and  $\text{MnCl}_3\text{-T}_\text{C}\text{-13-aSiCNR-center}$ . The computed results reveal that all of these configurations with parallel coupling are lower in energy than the corresponding ones with antiparallel coupling (Table S1†), indicating that parallel coupling between two neighboring  $\text{MnCl}_3$  units can be more stable. Therefore, all the computed results based on the supercell containing one  $\text{MnCl}_3$  should be reliable.

## 4 Conclusions

On the basis of first-principles computations, we have performed a detailed theoretical study on the structures, and the electronic and magnetic properties of modified zSiCNR and aSiCNR systems by adsorbing the magnetic superhalogen  $\text{MnCl}_3$ , which has a strong electron-withdrawing ability and a large intrinsic magnetic moment. The following intriguing findings are reported:

(1) when adsorbing  $\text{MnCl}_3$  at the ribbon center, magnetism can be introduced in the substrate SiCNR, and simultaneously an electron transfer process can be induced from SiCNR to  $\text{MnCl}_3$ , leading to an evident increase of electrostatic potential in the ribbon plane, like applying an electric field. As a result, the magnetic degeneracy of pristine zSiCNR can be broken and the strong ferromagnetic metallicity can be observed, while the nonmagnetic semiconductor aSiCNR can be transformed to exhibit a robust ferromagnetic half-metallicity.

(2) When moving  $\text{MnCl}_3$  from the center to the edge, the ferromagnetic metallicity can be changed to a robust ferromagnetic half-metallicity in the modified zSiCNR system, while the ferromagnetic half-metallicity can be converted into ferromagnetic SGS behavior in the modified aSiCNR system. Clearly, the adsorption site of  $\text{MnCl}_3$  has an important effect on the electronic and magnetic behaviors in the joint systems.

(3) Independent of the ribbon width, the robust ferromagnetic half-metallic or SGS behavior can be sustained in the  $\text{MnCl}_3$ -modified zSiCNR and aSiCNR systems at the edge, respectively.

(4) All of these new  $\text{MnCl}_3$ -modified SiCNR systems can exhibit large adsorption energies in the range of  $-1.430$  to  $-3.915$  eV, indicating they possess high structure stabilities.

Undoubtedly, adsorbing the magnetic superhalogen  $\text{MnCl}_3$  can be a new strategy to effectively modulate the electronic and magnetic properties of zSiCNR and aSiCNR systems. These intriguing findings can be advantageous for promoting the practical application of excellent SiC-based nanomaterials in spintronics and multifunctional nanodevices.

## Conflicts of interest

There are no conflicts to declare.

## Acknowledgements

This work was supported in China by NSFC (21673093, 21673094, 21373099 and 21573090), Science and Technology Research Program of Education Department of Jilin Province (JJJH20170780KJ and [2015] No. 465), and Jilin Province Science and Technology Development Plan (20170101175JC and 20150101005JC). We acknowledge the Computing Center of Jilin Province and the High Performance Computing Center (HPCC) of Jilin University for supercomputer time.

## References

- 1 K. S. Novoselov, A. K. Geim, S. V. Morozov, D. Jiang, Y. Zhang, S. V. Dubonos, I. V. Grigorieva and A. A. Firsov, *Science*, 2004, **306**, 666–669.
- 2 K. S. Novoselov, D. Jiang, F. Schedin, T. J. Booth, V. V. Khotkevich, S. V. Morozov and A. K. Geim, *Proc. Natl. Acad. Sci. U. S. A.*, 2005, **102**, 10451–10453.
- 3 M. I. Katsnelson and K. S. Novoselov, *Solid State Commun.*, 2007, **143**, 3–13.
- 4 S. V. Morozov, K. S. Novoselov, M. I. Katsnelson, F. Schedin, D. C. Elias, J. A. Jaszczak and A. K. Geim, *Phys. Rev. Lett.*, 2008, **100**, 016602.
- 5 C. Lee, X. D. Wei, J. W. Kysar and J. Hone, *Science*, 2008, **321**, 385–388.
- 6 D. Rodrigo, A. Tittl, O. Limaj, F. Abajo, V. Pruneri and H. Altug, *Light: Sci. Appl.*, 2017, **6**, e16277.
- 7 Y. Abate, S. Gamage, Z. Li, V. Babicheva, M. H. Javani, H. Wang, S. B. Cronin and M. I. Stockman, *Light: Sci. Appl.*, 2016, **5**, e16162.
- 8 Y.-W. Son, M. L. Cohen and S. G. Louie, *Nature*, 2006, **444**, 347–349.
- 9 H. Y. Lv, W. J. Lu, J. Y. Li, R. C. Xiao, M. J. Wei, P. Tong, X. B. Zhu and Y. P. Sun, *RSC Adv.*, 2017, **7**, 33408–33412.
- 10 Y. Y. Sun and S. B. Zhang, *J. Chem. Phys.*, 2016, **145**, 021102.
- 11 Y. F. Li, Z. Zhou, P. W. Shen and Z. F. Chen, *ACS Nano*, 2009, **3**, 1952–1958.
- 12 W. Chen, Y. H. Sun, J. Guan, Q. Wang, X. R. Huang and G. T. Yu, *RSC Adv.*, 2015, **5**, 53003–53011.
- 13 M. M. Monshi, S. M. Aghaei and I. Calizo, *RSC Adv.*, 2017, **7**, 18900–18908.
- 14 J. Guan, W. Chen, Y. F. Li, G. T. Yu, Z. M. Shi, X. R. Huang, C. C. Sun and Z. F. Chen, *Adv. Funct. Mater.*, 2013, **23**, 1507–1518.
- 15 J. Xiao, Z. L. Ye, Y. Wang, H. Y. Zhu, Y. Wang and X. Zhang, *Light: Sci. Appl.*, 2016, **4**, e366.
- 16 V. V. Ilyasov, C. V. Nguyen, I. V. Ershov and N. N. Hieu, *RSC Adv.*, 2015, **5**, 49308–49316.
- 17 P. Jiang, X. X. Tao, H. Hao, L. L. Song, X. H. Zheng, L. Zhang and Z. Zeng, *2D Mater.*, 2017, **4**, 035001.
- 18 X. H. Zheng, X. B. Chen, L. Zhang, L. T. Xiao, S. T. Jia, Z. Zeng and H. Guo, *2D Mater.*, 2017, **4**, 025013.
- 19 G. Kelner and M. Shur, in *Properties of Silicon Carbide*, ed. G. L. Harris, INSPEC, Institution of Electrical Engineers, London, 1995.



- 20 M. Mehregany, C. A. Zorman, S. Roy, A. J. Fleischman and N. Rajan, *Int. Mater. Rev.*, 2000, **45**, 85–108.
- 21 M. Willander, M. Friesel, Q. U. Wahab and B. Straumal, *J. Mater. Sci.: Mater. Electron.*, 2006, **17**, 1–25.
- 22 A. A. Lebedev, *Semicond. Sci. Technol.*, 2006, **21**, R17–R34.
- 23 G. D. Zhan, J. D. Kuntz, R. G. Duan and A. K. Mukherjee, *J. Am. Ceram. Soc.*, 2004, **87**, 2297–2300.
- 24 T. Narushima, T. Goto, T. Hirai and Y. Iguchi, *Mater. Trans., JIM*, 1997, **38**, 821–835.
- 25 S. Z. Wang, L. Y. Xu, B. Y. Shu, B. Xiao, J. Y. Zhuang and E. W. Shi, *J. Inorg. Mater.*, 1999, **14**, 527–534.
- 26 K. Watari, *J. Ceram. Soc. Jpn.*, 2001, **109**, S7–S16.
- 27 H. Zhang, W. Ding, K. He and M. Li, *Nanoscale Res. Lett.*, 2010, **5**, 1264–1271.
- 28 G. C. Xi, Y. Y. Peng, S. M. Wan, T. W. Li, W. C. Yu and Y. T. Qian, *J. Phys. Chem. B*, 2004, **108**, 20102–20104.
- 29 I. A. Salama, N. R. Quick and A. Kar, *J. Appl. Phys.*, 2003, **93**, 9275–9281.
- 30 R. Wu, L. Wu, G. Yang, Y. Pan, J. Chen, R. Zhai and J. Lin, *J. Phys. D: Appl. Phys.*, 2007, **40**, 3697–3701.
- 31 H. J. Li, Z. B. He, Y. H. Chu, L. H. Qi and Q. G. Fu, *Mater. Lett.*, 2013, **109**, 275–278.
- 32 Y. Ding and Y. Wang, *Appl. Phys. Lett.*, 2012, **101**, 013102.
- 33 L. Sun, Y. F. Li, Z. Y. Li, Q. X. Li, Z. Zhou, Z. F. Chen, J. L. Yang and J. G. Hou, *J. Chem. Phys.*, 2008, **129**, 174114.
- 34 J. Guan, G. T. Yu, X. L. Ding, W. Chen, Z. M. Shi, X. R. Huang and C. C. Sun, *ChemPhysChem*, 2013, **14**, 2841–2852.
- 35 J.-P. Colinge and C. A. Colinge, *Physics of semiconductor devices*, Kluwer Academic Publishers, Boston, 2002.
- 36 A. Castellanos-Gomez, *J. Phys. Chem. Lett.*, 2015, **6**, 4280–4291.
- 37 J. Guan, W. Chen, X. J. Zhao, G. T. Yu, X. R. Huang and C. C. Sun, *J. Mater. Chem.*, 2012, **22**, 24166–24172.
- 38 P. Lou and J. Y. Lee, *J. Phys. Chem. C*, 2009, **113**, 21213–21217.
- 39 F.-L. Zheng, Y. Zhang, J.-M. Zhang and K.-W. Xu, *Phys. Status Solidi B*, 2011, **248**, 1676–1681.
- 40 X. L. Ding, G. T. Yu, X. R. Huang and W. Chen, *Phys. Chem. Chem. Phys.*, 2013, **15**, 18039–18047.
- 41 W. Chen, H. Zhang, X. L. Ding, G. T. Yu, D. Liu and X. R. Huang, *J. Mater. Chem. C*, 2014, **2**, 7836–7850.
- 42 D. Liu, G. T. Yu, Y. H. Sun, X. R. Huang, J. Guan, H. Zhang, H. Li and W. Chen, *Phys. Chem. Chem. Phys.*, 2015, **17**, 941–950.
- 43 X. P. Shen, G. T. Yu, Z. S. Zhang, J. W. Liu, H. Li, X. R. Huang and W. Chen, *J. Mater. Chem. C*, 2017, **5**, 2022–2032.
- 44 S. N. Khanna and P. Jena, *Phys. Rev. Lett.*, 1992, **69**, 1664–1667.
- 45 S. N. Khanna and P. Jena, *Phys. Rev. B: Condens. Matter Mater. Phys.*, 1995, **51**, 13705–13716.
- 46 S. Aoyagi, E. Nishibori, H. Sawa, K. Sugimoto, M. Takata, Y. Miyata, R. Kitaura, H. Shinohara, H. Okada, T. Sakai, Y. Ono, K. Kawachi, K. Yokoo, S. Ono, K. Omote, Y. Kasama, S. Ishikawa, T. Komuro and H. Tobita, *Nat. Chem.*, 2010, **2**, 678–683.
- 47 M. Shibuta, T. Ohta, M. Nakaya, H. Tsunoyama, T. Eguchi and A. Nakajima, *J. Am. Chem. Soc.*, 2015, **137**, 14015–14018.
- 48 J. U. Reveles, P. A. Clayborne, A. C. Reber, S. N. Khanna, K. Pradhan, P. Sen and M. R. Pederson, *Nat. Chem.*, 2009, **1**, 310–315.
- 49 C. Y. Tu, G. T. Yu, G. H. Yang, X. G. Zhao, W. Chen, S. C. Li and X. R. Huang, *Phys. Chem. Chem. Phys.*, 2014, **16**, 1597–1606.
- 50 A. C. Reber, S. N. Khanna and A. W. Castleman, *J. Am. Chem. Soc.*, 2007, **129**, 10189–10194.
- 51 S. J. Wang, Y. Li, Y. F. Wang, D. Wu and Z. R. Li, *Phys. Chem. Chem. Phys.*, 2013, **15**, 12903–12910.
- 52 P. Jena, *J. Phys. Chem. Lett.*, 2015, **6**, 1119–1125.
- 53 M. M. Wu, H. P. Wang, Y. J. Ko, Q. Wang, Q. Sun, B. Kiran, A. K. Kandalam, K. H. Bowen and P. Jena, *Angew. Chem., Int. Ed.*, 2011, **50**, 2568–2572.
- 54 Y. W. Li, S. H. Zhang, Q. Wang and P. Jena, *J. Chem. Phys.*, 2013, **138**, 054309.
- 55 H. M. Zhao, J. Zhou, H. Fang and P. R. Jena, *ChemPhysChem*, 2016, **17**, 184–189.
- 56 X. L. Wang, *Phys. Rev. Lett.*, 2008, **100**, 156404.
- 57 G. Kresse and J. Hafner, *Phys. Rev. B: Condens. Matter Mater. Phys.*, 1993, **47**, 558–561.
- 58 G. Kresse and J. Furthmüller, *Comput. Mater. Sci.*, 1996, **6**, 15–50.
- 59 G. Kresse and J. Hafner, *Phys. Rev. B: Condens. Matter Mater. Phys.*, 1994, **49**, 14251–14269.
- 60 G. Kresse and J. Furthmüller, *Phys. Rev. B: Condens. Matter Mater. Phys.*, 1996, **54**, 11169–11186.
- 61 P. E. Blöchl, *Phys. Rev. B: Condens. Matter Mater. Phys.*, 1994, **50**, 17953–17979.
- 62 J. P. Perdew, K. Burke and M. Ernzerhof, *Phys. Rev. Lett.*, 1996, **77**, 2865–2868.
- 63 S. Grimme, *J. Comput. Chem.*, 2006, **27**, 1787–1799.
- 64 J. P. Perdew, J. A. Chevary, S. H. Vosko, K. A. Jackson, M. R. Pederson, D. J. Singh and C. Fiolhais, *Phys. Rev. B: Condens. Matter Mater. Phys.*, 1992, **46**, 6671–6687.
- 65 S. Dutta, A. K. Manna and S. K. Pati, *Phys. Rev. Lett.*, 2009, **102**, 096601.
- 66 G. T. Yu, D. Liu, W. Chen, H. Zhang and X. R. Huang, *J. Phys. Chem. C*, 2014, **118**, 12880–12889.
- 67 W. Chen, Y. F. Li, G. T. Yu, C. Z. Li, S. B. B. Zhang, Z. Zhou and Z. F. Chen, *J. Am. Chem. Soc.*, 2010, **132**, 1699–1705.

